Demonstration of a Rayleigh-Brillouin scattering spectrometer with high spectral resolution for rapid gas temperature detection

HONGDA YAN,[1] TAO WU,[1,*] SIHAO PI,[1] QIANG WU,[2] CHENWEN YE,[1] XINGDAO HE[1]

[1]*Key Laboratory of Nondestructive Test (Ministry of Education), Nanchang Hangkong University, Nanchang, 330063, China*
[2]*Department of Mathematics, Physics and Electrical Engineering, Northumbria University, Newcastle upon Tyne, NE1 8ST, UK*
** Corresponding author: wutccnu@nchu.edu.cn*

Received XX Month XXXX; revised XX Month, XXXX; accepted XX Month XXXX; posted XX Month XXXX (Doc. ID XXXXX); published XX Month XXXX

A novel Rayleigh-Brillouin scattering (RBS) spectrometer based on a virtually-imaged phased array (VIPA) with high spectral resolution is proposed for rapid gas temperature detection. CO_2 RBS spectra at gas pressure of 0.5-4 bar were acquired with a spectrum acquisition time of 10 s, and temperature inversion analysis was performed using TENTI S6 model. The root-mean-square error (RMSE) of the RBS profile fitting is less than 2.95% and the maximum absolute error of temperature inversion is less than 2.45 K. Compared with traditional methods, this method has low RBS signal loss and short acquisition time without frequency scanning process, which is more conductive to real-time detection applications.

The temperature of gases is an important physical parameter. It is essential to obtain detailed atmospheric temperature information below one standard atmospheric pressure to retrieve other atmospheric properties such as wind, relative humidity and trace gas concentrations [1]. It also important to measure high temperature gases at the elevated pressures found in combustion device [2]. Therefore, it is of great significance to realize real-time detection of temperature over a larger range of pressures. Due to its large scattering cross section and hence strong scattering signal, Rayleigh-Brillouin scattering (RBS) is an important type of light scattering, which has wide applications in the fields of environmental monitoring, defense industry and space engineering, etc [3]. In 2014 [4] and 2021 [5] Benjamin Witschas' team reported the use of the RBS method to measure the temperature of the atmosphere at altitudes of 2-15.3 km and surface to 10.5 km, respectively. The former results showed a temperature difference of up to 5 K within the boundary layer with an error of less than 2.5 K above the boundary layer under cloud-free conditions, and the latter temperature inversion error was less than 2 K. In 2017, Kun Liang *et al.* analyzed RBS spectral lines in the stratosphere and troposphere relevant to the Earth's atmosphere and atmospheric liDAR missions and validated them with air and nitrogen, and the absolute difference of the results was less than 3 K [6]. In 2019, Jingcheng Shang *et al.* investigated in detail the effect of Mie scattering on the temperature inversion of the RBS spectral profiles. Experiments were conducted at different temperatures and pressures using nitrogen mixed with aerosol experiments and the results show that the absolute error of temperature inversion is less than 3 K [7].

Current methods for the acquisition of RBS profiles in the laboratory are mainly based on using a high-finesse scanning Fabry–Perot interferometer (FPI), which guarantees high spectral resolution of RBS profiles. However, the low scattering intensity of RBS penetrated through FPI makes it difficult to obtain high signal-to-noise ratio (SNR) spectra. So a significant amount of time, ranging from tens of minutes to hours, is indispensable for the determination of high SNR spectra and then accurate gas temperature. A high-SNR RBS spectrum, for example, was acquired after spending 1.8 h at 3 bar by Ziyu Gu *et al.* in 2012 [8]. Yuanqing Wang *et al.* in 2019 acquired the RBS spectra of CO_2 gas at 1 bar in a typical time of about 3 h [9]. Furthermore, it is not possible to maintain perfectly steady conditions for such long durations in some practical applications. To improve the acquisition time of gas temperature in the field, low-Finesse FPI and Fizeau interferometer are employed. Benjamin Witschas et al. used a FPI with a low finesse of 6.4 to resolve RBS profiles, and the sampling of the entire RB line shape required at least 14 mins [4-5]. Jiaqi Xu et al. [10] proposed to utilize a Fizeau interferometer with the reflectivity of 80% and free spectral range (FSR) of 8.4 GHz as a frequency discriminator for imaging detection without any scanning process. In order to improve coupling efficiency and then temporal resolution, a multimode fiber with core diameter of 50 μm was used, resulting in a low finesse of 10. Temperature inversion using LiDAR data with an observation time of 5 min and a vertical resolution of 0.3 km was conducted. The results showed that inverted temperature error is less than 3 K in the altitude range of 4.0 km to 9.2 km.

Whether a FP/Fizeau interferometer is used, most of the light energy of the scattered light is reflected by coated reflective film, resulting in a weak scattered signal collected by a detector. A practical compromise, between coupling efficiency and the finesse of the FP/Fizeau interferometer must be considered. Thus, there is

a need for a more sensitive frequency discriminator with high optical coupling efficiency and spectral resolution. Virtually-imaged phased array (VIPA) is an interference-based optical element similar to the FP Etalon or Fizeau wedge. The VIPA consists of two parallel surfaces, and the two surfaces are both coated with ultra-high reflective dielectric. All the incident light is coupled into the VIPA via a small entrance window having an antireflection coating. The finesse and hen spectral resolution is related to the number of reflections between the two surfaces. The VIPA offers the possibility to achieve high throughput intensity (typical 50% to 70%) and high finesse (>40) [11-13]. In recent years, they have been widely used in biological studies based on Brillouin scattering [14], velocity fine measurements based on Doppler shift [15], and ultrafine spectral studies [16]. The presence of an incident window coated with antireflection makes the coupling efficiency high. Combined with the diffraction grating to realize the orthogonal decomposition of the spectrum, it provides an idea to realize the fast measurement of RBS spectral lines without wavelength scanning. To the best of our knowledge, no VIPA-based spectral measurement system has been reported for gas temperature inversion based on RBS.

In this letter, we proposed a gas temperature detection method using a VIPA and demonstrate an experimental setup with low insertion loss and short acquisition time by measuring the RBS spectra of CO_2, which provides several experimental spectra in the gas pressure range from 0.5-4 bar. And the experimental temperature was inverted based on measured RBS spectra.

Fig. 1 shows a schematic diagram of the complete experimental system. The operating wavelength of the frequency-doubled CW diode-pumped Nd:YVO4 laser is 532.23 nm with a line-width of less than 5 MHz and an average output power of 8 W. The main laser beam was split into two beams by a 95:5 beam splitter, where 95% of the laser was adjusted to the direction by mirrors M1 and M2 and passed through a hollow track, and was injected into the gas scattering cell through the entrance window in order to excite spontaneous RBS of the gas. After passing through the gas scattering cell, the excess beam transmitted through the output window is captured by an optical trap. 5 % of the laser beam is redirected by the mirror M3, attenuated by a factor of 100, and then injected into a 105 μm multimode fiber by the lens L5 (f=100mm) as a reference light to calibrate a series of optical components for VIPA and spectral line measurements. During measurement, the reference fiber at the input end of the fiber collimator needs to be changed to the signal fiber.

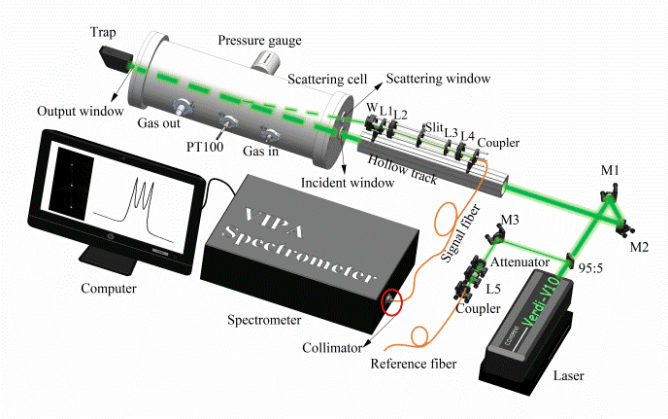

Fig.1. 3D view of the developed RBS spectrometer. M1, M2, M3: mirror; L1, L2, L3, L4: lens; W: prism set.

The signal light in the scattering direction of 167°4′ is emitted through the scattering window of the gas scattering cell, and collected by the prism set W (composed of two circular wedge prisms with a wedge angle of 11°22′, with each lens providing 6° of deflection, and the two combinations providing up to 12° of deflection), which made it to be deflected to the horizontal direction. The long-focal-length lens L1 (f = 750 mm) converts it into parallel light in an approximate way. L2 (100 mm), L3 (100 mm), and the adjustable slit constituted a spatial filter for the spatial filtration of the received scattered light. The light is then converged into an optical fiber with a core diameter of 105 μm through the lens L4 (f=60 mm) and transmitted to a fiber collimator for collimation and then injected into a VIPA-based spectrometer for spectral separation and imaging on a CCD, and finally saved and analyzed by a computer.

The gas scattering cell with a diameter of 200 mm and a long of 600 mm is large enough to encompass the entire measurement volume of the scattering light receiving configuration, making it suitable for simulating gas environments. The front panel of the scattering cell has a centered entrance window and a scattering window in the upper center. There is an output window in the center of the rear panel. All windows are 30 mm in diameter and have an anti-reflective coating. Since stray light from the wall of the scattering cell is important, more light- shielding elements are placed where necessary. The cells are wrapped with black matte aluminum foil to reduce the effect of stray light on the scattered signal. The temperature at the detection point in the gas cell is monitored by a PT100 with an accuracy of 0.01 K and captured by a data acquisition module and displayed by a computer. Gas to be measured is supplied from a high-pressure cylinder and passes through a gas filter to filter out aerosol particles with a diameter of greater than 3 nm. Two different devices are used for gas pressure control. Low pressure is realized by a diaphragm pump. The low-pressure environment up to 1000 mbar is monitored by a temperature-stabilized capacitive diaphragm vacuum gauge with an accuracy of 0.01 mbar and displayed in real-time by a pressure display module. High pressures above 1000 mbar are monitored and displayed by a pressure gauge with an accuracy of 1 mbar. Excess gas is discharged to the atmosphere through a three-way valve. Temperature and pressure sensors, filters and diaphragm pump are connected though standard KF flange connections on the vacuum tube using clamps.

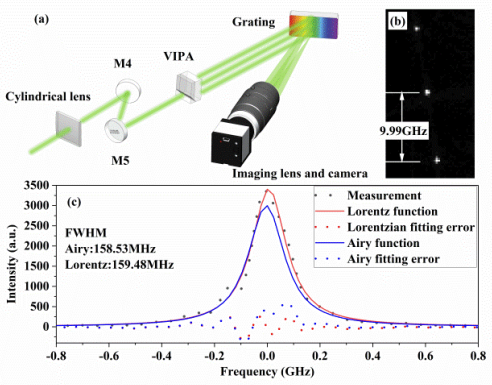

Fig. 2 (a) Details for the VIPA-based spectrometer, (b) IRF image on the CCD camera, (c) Results of fitting the instrument response function using Lorentzian (red line) and Airy function (blue line).

A detailed diagram of the VIPA-based spectrometer is given schematically in Fig. 2 (a). It consists of VIPA, diffraction grating, lens, mirrors and CCD. The light collimated by the fiber optic collimator is focused to the entrance window of the VIPA by a cylindrical lens with a focal length of 300 mm. The long focal length of the cylindrical lens enables to increase output signal intensity by reducing the angular spread of the beam within the VIPA, thus limiting the spectral energy to fewer out- put modes [17]. Two mirrors M4 and M5 inserted in the middle realize the folding of the optical path to reduce the overall size and facilitate the adjustment of the direction of the optical path. The VIPA used (Lightmachinery Inc.) has an FSR of 10 GHz at 532 nm. The reflectivity of front and back surface are R1 > 99.9% and R2 > 95%, respectively, and the small entrance window on the light input side has an anti-reflective coating. The spectrum information-carrying spectra is dispersed by the VIPA and diffraction grating in directions orthogonal to each other, and then focused onto the image plane of a CCD (4.54 μm/pixel) through an imaging lens with a focusing distance of 300 mm. The long focal length of the imaging lens enhances the size of the imaging spectrum, effectively improves the spectral resolution of the spectrometer [17]. The spectral structure is converted into voltage value and it is mapped onto a two-dimensional plane, and then processed by a computer to obtain the RBS spectra. There is an isolation box surrounding the collection optics to suppress stray light.

The instrument response function (IRF) of a system is an important parameter for gas temperature inversion. Therefore, the IRF of the system developed in this paper must be considered. Without considering the influence of the laser line-width (<5 MHz), the IRF is mainly determined by the VIPA-based spectrometer used. When using the reference light to measure the IRF of the system, the image displayed on the CCD camera is a column of bright spots as shown in Fig. 2 (b). The distance between each adjacent two bright spots is the FSR of the VIPA. Lorentzian [18] and Airy function [19] have been mentioned for fitting the IRF of VIPA spectrometer. Two methods are used and compared here. The Lorentzian fitting error shown in Fig. 2 (c) is lower than Airy function fitting result. So a FWHM of 159.48 MHz got by Lorentzian fitting is used, and a high finesse of 62 is achieved.

In order to verify the functionality of the proposed technique and characterize the achievable accuracy and precision, measurements were performed using CO_2 gas at a temperature of approximately 295 K in a gas pressure range of 0.5-4 bar. It is worth noting that the pressure is not limited to this range and higher or lower pressure ranges are also feasible. All demonstrated spectra were averaged using 10 individual spectra profiles with a single acquisition time of 1000 ms. The results are shown in Fig. 3 (a).

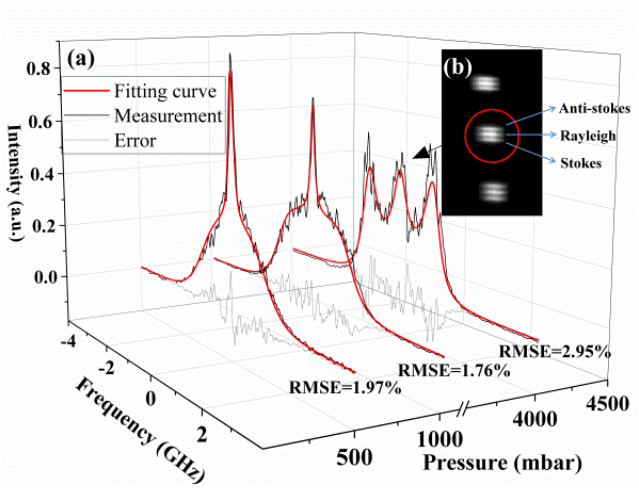

Fig.3. (a) RBS spectrum measured from 0.5 bar to 4 bar, (b) RBS spectral profile image on the CCD camera at gas pressure of 4 bar.

It can be seen in Fig. 3 (a) that, in the low-pressure range, the Rayleigh peak in the center of the spectrum dominates, while at higher pressure range, the Brillouin peak is separated from the Rayleigh peak. Fig. 3 (b) shows the RBS spectral profile image on the CCD camera at gas pressure of 4 bar. Each larger bright spot contains three fringes corresponding to the anti-stokes, Rayleigh and stokes peaks. This phenomenon on the CCD camera also suggests that the Rayleigh and Brillouin peaks can be completely distinguished at higher pressure range. A high-purity CO2 gas (CO2 ⩾ 99.999%) was used in the experiment. However, the narrow band spectral structure was found superimposed on the center of the Rayleigh peaks at low pressure, which may be caused by stray light in the scattering cell and window. The magnitude of the impact of this spectral structure on the final results needs to be analyzed in detail subsequently.

The TENTI S6 model is currently an effective method for fitting RBS spectral lines. Typically, experimentally measured spontaneous RBS spectra are the result of convolution of the ideal spontaneous RBS signal with the system IRF. It's precisely because the spectrum collected contains the visible narrow-band spectral structure, that the delta function describing it was added. Thus the actual captured RBS profiles can be described as:

$$M(p,T,f)=\left[I_{mol}\bullet S_{mol}(p,T,f)+I_{del}\bullet S_{del}(p,T,f)\right]*W(f) \quad (1)$$

where $*$ is the convolution operation, I_{mol} is the RBS signal intensity of the gas molecule, $S_{mol}(p, T, f)$ is the RBS spectral line normalized to the S6 model, I_{del} is the laser diffuse reflection intensity, $S_{del}(p, T, f)$ is the delta function and $W(f)$ is the IRF of the VIPA.

The fitting results are shown as red lines in Fig. 3 (a). In order to quantitatively characterize the measured differences between the theoretical and actual spectra, the RMSE was calculated using the following equation:

$$RMSE=\sqrt{\frac{\sum_{i=1}^{N}\left[I_m(f_i)-I_i(f_i)\right]^2}{N}} \quad (2)$$

Where $I_m(f_i)$ is the intensity of measured RBS profiles, $I_i(f_i)$ is the intensity of the Tenti S6 model, and N is the number of data.

The RMSE of the fitting results for all three spectra is also shown in Fig. 3 (a) and the maximum RMSE is less than 2.95%. The fitting

errors mostly exist at the peaks, which are related to the existence of the narrow-band structure and the difficulty of the program in fitting the peaks.

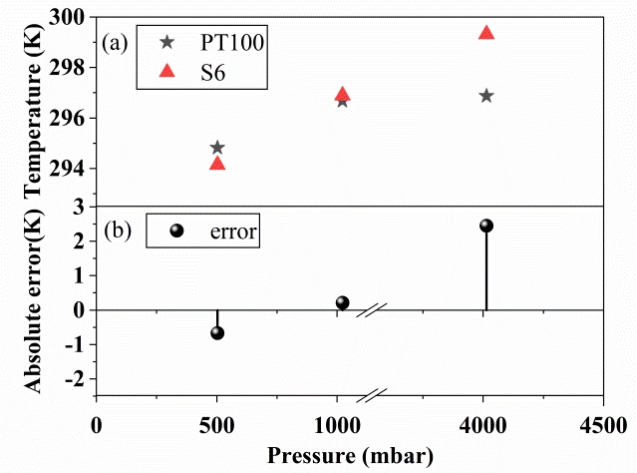

Fig.4. Temperature retrieved from RBS profile. (a) retrieved temperature values (red triangle) and PT100 measured values (black star), (b) the differences between them.

During the temperature inversion, the intensity, temperature and Mie contribution are variable, while the other parameters in the S6 model, including pressure, are fixed. We use the least squares method to find the best fit to determine the temperature value.

The temperature values inverted from the RBS spectral line shown in Fig. 3 (a) are shown as red values (triangle symbols) in Fig. 4 (a), and the temperatures at the time of the experiments were recorded by a PT100 and shown as gray values (pentagrams) in Fig. 4 (a). The absolute temperature error is shown in Fig. 4 (b).

The temperature absolute errors of the three RBS spectral inversions are 0.67 K, 0.21 K, and 2.45 K, respectively, and the average absolute error is 1.11 K. It is worth noting that when future applications are extended to lower pressures, the measured RBS signal level will be further attenuated and the narrow-band spectral structure will dominant. The intensity of the narrow-band light will overpower the scattered light, while the inversion error of the temperature will be increased. On the contrary, when under high-pressure conditions, the gas RBS scattering intensity is high enough for high SNR of RBS spectra and the Brillouin peaks evidently separated from the Rayleigh peaks, which may cause the Brillouin peak fitting to be more difficult, and the influence of the IRF on the fitting becomes more pronounced. In addition, although there is still some difference between the temperature inversion value and the exact value, the error can be further reduced if more error factors, such as laser drift, etc., are considered, and correction and optimization are performed in the experiment, in the subsequent studies. Overall, with this measurement, it is verified that the proposed VIPA-based gas temperature detection method and experimental setup are feasible and the temperature inversion works properly, at least within the experimental pressure range.

In this letter, a novel VIPA-based RBS spectrometer with high spectral resolution for rapid gas temperature detection is presented, which is characterized by low insertion loss, and short spectral acquisition time. Spectral profiles were detected with CO_2 pressure from 0.5 bar - 4 bar and the maximum deviation of the retrieved gas temperature is less than 2.45 K. Compared with existing scanning FPI schemes and Fizeau interferometer-based detection schemes , the demonstrated method in this paper is more conducive for real-time detection applications. In addition, the lack of movable components makes the technique promising even in harsh environments. We perform these measurements in CO2 because of its large scattering cross-section, and the ultimate goal is actually to measure the temperature in the atmosphere. When measuring the atmospheric temperature profiles, the setup will be modified by replacing continuous lasers and CCD with pulse lasers and ICCDs, respectively.

Funding. National Natural Science Foundation of China (Grant No. 61965013, 42175130, 41665001), the Key Program of Natural Science Foundation of Jiangxi Province, China (No. 20232ACB202002), Training Funding Project of High-Level and High-Skill Leading Talent of Jiangxi Province, China and Open Basic Research Program of Laboratory of Intense Dynamic Loading and Effect, China (IDEL1905).

Disclosures. The authors declare no conflicts of interest.

Data availability. Data underlying the results presented in this paper are not publicly available at this time but may be obtained from the authors upon reasonable request.

References

1. B. Witschas, Z. Gu, and W. Ubachs, Opt. Express **22**, 29655 (2014).
2. H. Park, S. Bae, H. Do, *et al.*, Phys. Fluids **34**, 081701(2022).
3. P. Zhang, J. Xu, R. Zhang, *et al.*, IEEE Access **8**, 22964 (2020).
4. B. Witschas, C. Lemmerz, and R. Oliver, Opt. Lett. **39**, 1972 (2014).
5. B. Witschas, C. Lemmerz, O. Lux, *et al.*, Opt. Lett. **46**, 4132 (2021).
6. K. Liang, J. Xu, P. Zhang, *et al.*, Sensors **17**, 1503 (2017).
7. J. Shang, T. Wu, C. Yang, *et al.*, Opt. Commun. **436**, 127 (2018).
8. Z. Gu, M. O. Vietez, E. J. van Duijn, *et al.*, Rev. Sci. Instrum. **83**, 053112 (2012)
9. Y. Wang, W. Ubachs, and W. van de Water, J. Chem. Phys. **150**, 154502 (2019).
10. J. Xu, B. Witschas, P. G. Kableka, *et al.*, Opt. Lett. **46**, 3320 (2021).
11. A. M. Weiner, Appl. Optics **51**, 8187(2012).
12. G. Scarcelli, and S. Yun, Opt. Express **19**, 10913(2011).
13. X. Zhu, D. Lin, Z. Hao, *et al.*, Astron. J. **160**, 135 (2020).
14. Y. Zhang, S. Wang, X. Zheng, *et al.*, Acta. Phys. Sin. **64**, 037801 (2015).
15. Y. Krishna, X. Luo, and G. Magnotti, Opt. Lett. **46**, 5252 (2021).
16. A. Durocher-Jean, H. Jean-Ruel, L. I. Dion-Bertrand, *et al.*, J. Phys. D Appl. Phys. **54**, 085204 (2021).
17. K. Teav, and A. M. Steinberg, P. Combust. Inst. **39**, 1425 (2023).
18. G. Yan, A. Bazir, J. Margueritat, *et al.*, Biomed. Opt. Express **11**, 6933(2020).
19. C. Ouyang, C. Xie, Y. Wu, *et al.*, Appl. Phys. Express **16**, 022003(2023).